LOSS-ANGLE MEASUREMENT

Dielectrics, in the most general sense, may be considered as the broad class of *nonmetals* from the standpoint of their interaction with electric and magnetic fields. Hence gases, liquids, and solids can all be included, both with respect to their ability to store electric and magnetic field energy, as well as the accompanying dissipative processes occurring in the material when placed in an electric or magnetic field. How these phenomena can be described macroscopically and interpreted from the standpoint of molecular theory, how they can be accurately measured, and what the properties of various materials are provides the groundwork for their use in the rapidly growing microelectronic applications that shape much of our world today.

In a more narrow sense, dielectric materials may be classified from basic principles of the *energy-band model* as electrical insulators. The energy-band model forms the basis for development of all components in solid-state electronics. This model shows that the possible energies of electrons in a crystal are grouped in a certain number of allowed energy bands separated from one another by forbidden energy bands. The position of the Fermi energy, or energy of the topmost filled electron level in the sequence of allowed and forbidden bands, permits a unified treatment of metals, semiconductors, and insulators. According to the energy-band model, matter becomes dielectric (a poor conductor of electricity) when the conduction band and the valence band are separated by an energy gap higher than 5 eV. At normal temperatures only a small number of electrons have sufficient thermal energy necessary to make a transition to the conduction band. When temperature increases, the transition probability increases and the electrical conductivity σ can be written as

$$\sigma = \sigma_0 e^{-W/k_B T} \tag{1}$$

where W is the activation energy of the conduction process, k_B is Boltzmann's constant (1.38062×10^{-23} J/K), and T is the absolute temperature. In general, Eq. (1) is valid for crystalline and amorphous dielectrics, as well as partially crystalline dielectrics such as polymers.

Materials, whether in the solid, liquid, or gaseous states, may be electrically nonlinear, anisotropic, inhomogeneous, and dispersive both with respect to frequency and temperature. Dissipation results from loss mechanisms that can differ in different types of materials. Because of all these complicating factors, both measurement technique and accuracy for evaluation of dielectric properties are requisite for physical understanding. Dielectric-loss-angle measurements reflect the different loss mechanisms occurring in a material placed in an electric field. This article addresses various measurement techniques for dielectric loss angle and permittivity evaluation of materials and is organized as follows:

- Electromagnetic characteristics of materials (constitutive equations, anisotropy, polar versus nonpolar materials, free charge versus bound charge, complex refractive index, polarization mechanisms, dispersion and relaxation processes)
- Permittivity and dielectric-loss-angle measurements (low-frequency complex impedance, free-space measurements for solids, liquids and gases, waveguide transmission and reflection techniques, resonance methods, and anisotropic material measurements)

ELECTROMAGNETIC CHARACTERISTICS OF MATERIALS

Physical Concepts Governing Electromagnetic Behavior

Any material is electromagnetically characterized by its permittivity ϵ (F/m), magnetic permeability μ (H/m), and electrical conductivity σ (S/m). Maxwell's equations, together with the constitutive equations relating field quantities in terms of material properties, completely govern electromagnetic wave propagation and behavior in that medium.

The constitutive equations for a linear, homogeneous, and isotropic medium may be expressed in the frequency domain as

$$\begin{aligned} \boldsymbol{B} &= \mu \boldsymbol{H} \\ \boldsymbol{J} &= \sigma \boldsymbol{E} \\ \boldsymbol{D} &= \epsilon \boldsymbol{E} \end{aligned} \tag{2}$$

where the magnetic induction $\boldsymbol{B}$ (Wb/m^2) is related to the magnetic field $\boldsymbol{H}$ (A/m) by the magnetic permeability, the current density $\boldsymbol{J}$ (A/m^2) is related to the electric field $\boldsymbol{E}$ (V/m) by the conductivity, and the dielectric displacement field $\boldsymbol{D}$ (C/m^2) is related to the electric field by the permittivity. Any deviation from linearity is usually included by making ϵ, μ, or σ field dependent. For anisotropic media, ϵ, μ, or σ is a second-rank tensor as opposed to just a scalar function of frequency or simply a constant. For inhomogeneous media, ϵ, μ, or σ is a function of spatial coordinates. Material dielectrics that are linear, isotropic, and homogeneous when placed in

J. Webster (ed.), *Wiley Encyclopedia of Electrical and Electronics Engineering*. Copyright © 1999 John Wiley & Sons, Inc.

an electric field at one frequency may not be isotropic or homogeneous when placed in an electric field at another frequency or under different temperature or pressure conditions. Similarly, dielectrics that behave linearly when placed in weak electric fields may not be linear in strong fields (or at high temperatures).

Anisotropy

When a dielectric is placed in an electric field $\boldsymbol{E}$, the material becomes polarized, and the dielectric displacement field is often written

$$\boldsymbol{D} = \epsilon_0 \boldsymbol{E} + \boldsymbol{P} \tag{3}$$

where $\boldsymbol{P}$ is defined as the electric polarization of the material (dipole moment per unit volume), and is related to the electric field as

$$\boldsymbol{P} = \epsilon_0 \chi \boldsymbol{E} \tag{4}$$

the proportionality constant χ is called the electric susceptibility, and the factor ϵ_0 (free-space permittivity equal to 8.854×10^{-12} F/m) is included in Eq. (3) to make χ dimensionless. Then Eq. (2) becomes

$$\boldsymbol{D} = \epsilon_0 (1 + \chi) \boldsymbol{E} \tag{5}$$

or

$$\boldsymbol{D} = \epsilon_0 \epsilon_r \boldsymbol{E} \tag{6}$$

where $\epsilon_r = 1 + \chi$ is called the complex permittivity of the medium relative to a vacuum. The presence of a dielectric always affects the ratio of $\boldsymbol{D}$ to $\boldsymbol{E}$ by a factor of ϵ_r. For *linear* materials the dipole moment induced in a dielectric by an external field $\boldsymbol{E}$ is directly proportional to $\boldsymbol{E}$. As long as the electric properties of the dielectric are independent of direction of the applied electric field, it is *isotropic;* that is, $\boldsymbol{P}$ and $\boldsymbol{E}$ are collinear. For an *anisotropic* material, however, the polarization (or charge separation) obtained when an electric field is applied along one coordinate axis will be different from that produced by the same field applied along a different coordinate axis. Quantitatively, this can be expressed by writing

$$\boldsymbol{P} = \epsilon_0 \overline{\overline{\chi}} \cdot \boldsymbol{E} \tag{7}$$

where $\overline{\overline{\chi}} = \chi_x \boldsymbol{ii} + \chi_y \boldsymbol{jj} + \chi_z \boldsymbol{kk}$ and χ_x, χ_y, χ_z are the principal components of the electric susceptibility tensor expressed in dyadic form. For isotropic materials $\chi_x = \chi_y = \chi_z$, and Eq. (7) reduces to Eq. (4). Equation (7) shows that $\boldsymbol{P}$ and $\boldsymbol{E}$ are not collinear when $\chi_x \neq \chi_y = \chi_z$ or when $\chi_x = \chi_y \neq \chi_z$ or when $\chi_x \neq \chi_y \neq \chi_z$ (for two- or three-dimensional anisotropy), so that the electric susceptibility tensor may, in general, be viewed as an operation that takes a vector $\boldsymbol{E}$ and converts it into a new vector $\boldsymbol{P}$ that is not collinear with $\boldsymbol{E}$.

Polar versus Nonpolar Materials

Dielectric materials may also be divided into one of two categories: *polar* and *nonpolar.* A nonpolar material (such as inert or rare gases) is simply one that contains no (equivalent) dipoles (or separation of charge) when the material is not in an electric field. A polar material, on the other hand, possesses permanent polarization, even in the absence of an electric field, due to its molecular structure. Polar materials have permanent dipole moments at the microscopic or molecular level. A common polar molecule is the water molecule whose equivalent dipole moment results from a 104° angle between the two OH^- anions; this can be contrasted with the CO_2 molecule, in which the individual moments of each CO pair cancel, yielding a zero permanent moment.

In general, any distribution of charge may be described in terms of its multipole moments (1). The relevance of this discussion to dielectric material properties is that the existence of permanent dipole moments on the molecular level gives rise to a type of polarization mechanism when an electric field is applied that is frequency-dependent. Without an applied electric field in the case of the water molecule, the individual molecular dipole moments point in random directions, so that macroscopically their vector sum vanishes. In the presence of the applied electric field $\boldsymbol{E}$, though, there is a pronounced tendency of the dipoles to line up in the direction of $\boldsymbol{E}$, creating an *orientational* polarization whose magnitude can be computed and measured (2).

Ferroelectric materials are those in which there is spontaneous alignment of electric dipole moments at the molecular level. This occurs in ferroelectric materials at the Curie temperature. The permittivity of a ferroelectric material is field-strength dependent, which allows ferroelectric materials to be used in a variety of nonlinear devices, such as piezoelectric transducers, voltage-controlled oscillators, varactors, tunable filters, and phase shifters.

Complex Material Constituent Properties

The solution of Maxwell's equations yields all of the quantities that describe the propagation of electromagnetic waves in terms of the propagation constant $\sigma = jk$, where k is the complex wavenumber defined by

$$k^2 = \omega\mu(\omega\epsilon - j\sigma) \tag{8}$$

for $\exp(+j\omega t)$ time dependence for angular frequency ω and time t.

In general, the constituent electrical properties may be written as complex quantities; that is, for $\exp(+j\omega t)$ time dependence

$$\begin{aligned} \epsilon &= \epsilon' - j\epsilon'' = (\epsilon_r' - j\epsilon_r'')\epsilon_0 = \epsilon_r\epsilon_0 \\ \sigma &= \sigma' + j\sigma'' \\ \mu &= \mu' - j\mu'' = (\mu_r' - j\mu_r'')\mu_0 = \mu_r\mu_0 \end{aligned} \tag{9}$$

where μ_0 is the free-space permeability equal to $4\pi \times 10^{-7}$ H/m. Each component of ϵ, σ, or μ (which for anisotropic materials are tensor matrices) is, in general, a complex quantity. The imaginary part of the propagation constant contains all necessary information about energy loss in a material medium during wave propagation. If magnetic properties are ignored, we may consider only the complex form of ϵ and σ in Eq. (8):

$$\omega\epsilon - j\sigma = \omega(\epsilon' - j\epsilon'') - j(\sigma' + j\sigma'') = (\sigma'' + \omega\epsilon') - j(\sigma' + \omega\epsilon'') \tag{10}$$

Here $\omega\epsilon' + \sigma''$ may be considered an effective permittivity and $\sigma' + \omega\epsilon''$ as an effective conductivity. The term $\sigma' + j\sigma''$ physically represents carrier transport due to Ohmic and Faraday diffusion mechanisms, whereas $\epsilon' - j\epsilon''$ represents dielectric relaxation mechanisms. From Eq. (10), the loss tangent is simply defined as

$$\tan\delta = \tan\left(\psi + \frac{\pi}{2}\right) \equiv \frac{\sigma' + \omega\epsilon''}{\sigma'' + \omega\epsilon'} \tag{11}$$

where ψ is the phase between $\boldsymbol{E}$ and $\boldsymbol{J}$. If there are no dielectric losses, $\epsilon'' \to 0$. Similarly, if there are no Faraday losses, $\sigma'' \to 0$; hence

$$\tan\delta = \frac{\sigma'}{\omega\epsilon'} \tag{12}$$

which describes losses physically due to Ohmic conductivity.

Distinction between Ohmic Conductivity (σ') and Dielectric Loss Factor (ϵ'') or between Faraday Diffusion Transport (σ'') and In-Phase Polarization Phenomena (ϵ')

It is often stated that it is artificial to make distinctions between Ohmic carrier transport phenomena and dielectric loss characteristics of a material when that material is placed in a time-varying electric field. Actual dielectric measurements are indifferent to the underlying physical processes. To the extent, however, that physical and chemical processes are understood, distinctions can be made and materials designed to have certain electromagnetic characteristics.

The lack of distinction between two loss mechanisms from only measurement data can be seen by inspection of Eq. (11). Another way to see the relation between conductivity and the imaginary part of the permittivity is to write Ampere's law,

$$\nabla \times \boldsymbol{H} = \boldsymbol{J} + \frac{\partial \boldsymbol{D}}{\partial t} \tag{13}$$

where $\boldsymbol{J}$ is the conduction current in a material medium due to an applied electric field. For sinusoidal fields, Eq. (13) can be rewritten as

$$\begin{aligned}\nabla \times \boldsymbol{H} &= \sigma\boldsymbol{E} + \epsilon\frac{\partial \boldsymbol{E}}{\partial t} \\ &= (\sigma + j\omega\epsilon_0\epsilon_r)\boldsymbol{E} \\ &= j\omega\left[\epsilon_r' - j\left(\epsilon_r'' + \frac{\sigma}{\epsilon_0\omega}\right)\right]\epsilon_0\boldsymbol{E}\end{aligned} \tag{14}$$

Hence, without other physical information, a conductivity σ is equivalent to an imaginary part of ϵ given by

$$\epsilon_r'' = \frac{\sigma}{\omega\epsilon_0} \tag{15}$$

so an equivalent form of Eq. (12) is

$$\tan\delta = \frac{\epsilon''}{\epsilon'} = \frac{\text{(loss current)}}{\text{(charging current)}} \tag{16}$$

Time-Domain Dielectric Constitutive Equation

The permittivity ϵ in Eq. (2) is defined for a time-harmonic electromagnetic phasor field at a certain frequency ω. If the permittivity is independent of frequency, the relationship in the time domain is simply expressed by

$$\boldsymbol{D}(\boldsymbol{r}, t) = \epsilon\boldsymbol{E}(\boldsymbol{r}, t) \tag{17}$$

However, if the permittivity is a function of frequency, the temporal relationship is a Fourier transform of the product of $\epsilon(\omega)$ and $\boldsymbol{E}(\omega)$ and is therefore given by the convolution integral

$$\boldsymbol{D}(\boldsymbol{r}, t) = \int_{-\infty}^{t} h(t-\tau)\boldsymbol{E}(\boldsymbol{r}, \tau)\, d\tau \tag{18}$$

where

$$h(t) = \frac{1}{2\pi}\int_{-\infty}^{\infty} \epsilon(\omega)e^{j\omega t}\, d\omega \tag{19}$$

$$\boldsymbol{E}(\boldsymbol{r}, t) = \frac{1}{2\pi}\int_{-\infty}^{\infty} \boldsymbol{E}(\boldsymbol{r}, \omega)e^{j\omega t}\, d\omega \tag{20}$$

The medium whose permittivity is a function of frequency $\epsilon(\omega)$ is called dielectrically dispersive. Although, strictly speaking, all media are dispersive, a medium can often be treated as nondispersive within a frequency range used for a particular problem.

If a medium is linear but varies with time, the relationship between $\boldsymbol{D}$ and $\boldsymbol{E}$ cannot be expressed as the convolution integral, Eq. (18). The general relationship should then be given by

$$\boldsymbol{D}(\boldsymbol{r}, t) = \int_{-\infty}^{t} h(t, t-\tau)\boldsymbol{E}(\boldsymbol{r}, \tau)\, d\tau \tag{21}$$

Substitution of Eq. (20) into Eq. (21) yields

$$\boldsymbol{D}(\boldsymbol{r}, t) = \frac{1}{2\pi}\int_{-\infty}^{\infty} \epsilon(t, \omega)\boldsymbol{E}(\boldsymbol{r}, \omega)e^{j\omega t}\, d\omega \tag{22}$$

where $\epsilon(t, \omega)$ is the time-varying permittivity given by

$$\epsilon(t, \omega) = \int_{0}^{\infty} h(t, \tau)e^{j\omega\tau}\, d\tau \tag{23}$$

Time-varying media will not be discussed in this article.

Complex Refractive Index

For a nonabsorbing medium the refractive index is defined as c/u, where $c = 1/\sqrt{\mu_0\epsilon_0}$ is the velocity of propagation in free space and u is the phase velocity in the material ($c/\sqrt{\mu_r'\epsilon_r'}$). For a dielectrically lossy medium a *complex refractive index* $n - j\kappa$ is defined such that

$$n - j\kappa = \frac{c}{u} = \frac{ck}{\omega} \tag{24}$$

so that

$$n^2 - \kappa^2 = \epsilon_r'\mu_r' \tag{25}$$

and

$$2n\kappa = \frac{\sigma \mu_r'}{\epsilon_0 \omega} \tag{26}$$

where κ is the *absorption loss index.* The *absorption coefficient* α is related to the absorption loss index by $\alpha = 2\omega\kappa/c$. For a nonmagnetic material, Eqs. (25) and (26) may be solved for the refractive index and absorption loss index,

$$n = \frac{1}{\sqrt{2}} \left[\sqrt{(\epsilon_r')^2 + (\epsilon_r'')^2} + \epsilon_r' \right]^{1/2} \tag{27}$$

and

$$\kappa = \frac{1}{\sqrt{2}} \left[\sqrt{(\epsilon_r')^2 + (\epsilon_r'')^2} - \epsilon_r' \right]^{1/2} \tag{28}$$

For small dissipation, where $\tan\delta \sim \delta$, $n \simeq \sqrt{\epsilon_r'}$, and $\kappa \simeq \delta\sqrt{\epsilon_r'}/2 = \epsilon_r''/(2\sqrt{\epsilon_r'})$.

Quality Factor of Dielectric

The *quality factor* Q of a dielectric at frequency f is defined as the inverse of the loss tangent,

$$\begin{aligned} Q &= \frac{1}{\tan\delta} = \frac{\epsilon'}{\epsilon''} = \frac{\omega\epsilon' E_0^2}{\omega\epsilon'' E_0^2} \\ &= 2\pi f \frac{\frac{1}{2}\epsilon' E_0^2}{\frac{1}{2}\sigma E_0^2} \\ &= 2\pi \frac{\text{(average energy stored per half cycle)}}{\text{(energy dissipated per half cycle)}} \end{aligned} \tag{29}$$

The quality factor Q is used as a descriptive characteristic of any dielectric material.

Polarization Mechanisms Intrinsic to Materials. A pulse or "signal" of any specified *initial* form can be constructed by superposition of harmonic wave trains of infinite length and duration. The velocities with which the constant-phase surfaces of these component waves are propagated depend on the propagation constant or on the parameters ϵ, μ, and σ. If the medium is nonconducting and the quantities ϵ and μ are independent of the frequency of the applied field, the phase velocity is constant and the signal is propagated without distortion. The presence of a loss mechanism, however, yields a functional relation between the frequency and phase velocity, as well as between frequency and attenuation. Hence in a lossy or absorptive medium the harmonic components suffer relative displacements in phase in the direction of propagation, and the signal arrives at a distant point in a modified form. The signal is *dispersed* and attenuated, and a medium in which the phase velocity is a function of frequency f (or in which the complex dielectric constant ϵ is a function of frequency) is said to be electrically dispersive.

The quantity $\epsilon'(f; x, y, z)$ is a measure of the polarization of the material. There can be a number of different polarizing mechanisms, each having a characteristic relaxation frequency and dielectric dispersion centered around this relaxation frequency. At the relaxation frequency there is maximal

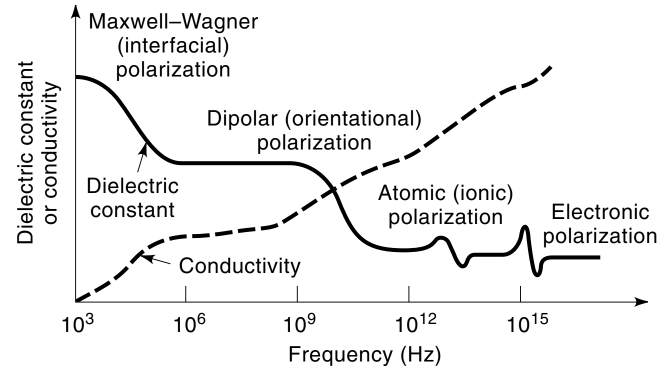

Figure 1. Dielectric dispersion for various types of polarization.

absorption. Figure 1 illustrates the dispersion of ϵ (and σ) that may be observed in materials in the frequency range 10^3 Hz to 10^{15} Hz. At the highest frequencies, the polarizing species in a material are the electrons. Electronic polarization occurs when an applied electric field causes a net displacement of the electron cloud of an atom with respect to its nucleus. At frequencies below about 10^{13} Hz, there is also a contribution from atomic polarization. Atomic polarization occurs in structures (molecules, solutions) in which atoms do not share electrons equally and electric fields displace the electron clouds preferentially towards the stronger binding atoms. It also occurs when charged atoms are displaced with respect to each other. Dipolar polarization, that is, the orientation of polar molecules (molecules with asymmetric charge distributions), occurs at frequencies below about 10^{10} Hz.

At frequencies below about 10^5 Hz, there are various types of charge polarization that may be collectively referred to as Maxwell–Wagner mechanisms (3,4). One of these, interfacial (space-charge) polarization, occurs when migrating charge carriers are trapped or impeded in their motion by local chemical or electric potentials, causing local accumulations of charge and a macroscopic field distortion. Another low-frequency mechanism that can occur is due to mixtures of materials having differing electrical properties (such as conducting spheres embedded in a dielectric). Several different equations are available to describe the resultant properties for various geometries of the embedded conductor (5–7). The common cause of these effects is the distributions of charge that occur at conductor–dielectric boundaries and the resultant action under applied electric fields that can yield very large low-frequency dielectric constants.

Still another dispersion mechanism for dielectric behavior at low frequencies, which is often distinguished from Maxwell–Wagner effects, is that which occurs in colloidal suspensions. Maxwell–Wagner effects occur when the charge around conducting particles in a dielectric medium is a thin coating that is much smaller than the particle dimensions; the charge responds to an applied electric field independent of the charge on nearby particles. In colloidal suspensions, on the other hand, the charge layer is on the same order of thickness or larger than the particle dimensions; hence it is affected by the charge distributions of adjacent particles. Colloidal polarization responses result in far higher low-frequency dielectric constants than those resulting from typical Maxwell–Wagner mechanisms, with dielectric constants on the order of 10^5 not uncommon.

Dispersion and Relaxation Processes in Materials. Polarization occurring in material media as a result of electromagnetic wave propagation is physically damped by either resonance or relaxation. Resonance is the state of a harmonic oscillator that is driven at its preferred frequency. Relaxation, on the other hand, is the state of a critically damped or overdamped oscillator. The characteristics of ϵ' and ϵ'' for these two differing types of dispersion and absorption processes are shown in Fig. 2.

At microwave frequencies, dipolar or orientation polarization phenomena principally occur. In this case, the frequency is sufficiently low so that the rotation of polar molecules has time to take place. At a frequency of $\omega = 1/\tau$, ϵ' decreases because the individual dipoles can no longer keep in step with the applied field. The relaxation time τ represents the time required for the dipoles to revert to a random distribution. This is a diffusion process that is represented by Fig. 2(a). Atomic and electronic polarization processes take place in the infrared and optical portion of the spectrum (1 THz and above) and lead to the resonance-type dispersion and absorption phenomenon represented by Fig. 2(b). A given medium may display any or all of these characteristic polarization phenomena, depending on its composition and molecular or atomic structure.

Relaxation processes are those observed in dielectric materials at microwave frequencies and below. Relaxation models are based on the general equation of charge motion,

$$\ddot{q} + (\mu\sigma)^{-1}\dot{q} + (\mu\epsilon)^{-1}q = 0 \tag{30}$$

where q is the charge and the overdot represents differentiation with respect to time. Another relaxation model is based on the diffusion of charged ions whose concentration is spatially variable. In this case

$$\begin{aligned}\frac{\partial^2}{\partial x^2}\overline{Q}(t;x,y,z) + \frac{\partial^2}{\partial y^2}\overline{Q}(t;x,y,z) + \frac{\partial^2}{\partial z^2}\overline{Q}(t;x,y,z) \\ = \frac{\partial^2\overline{Q}(t;x,y,z)}{\partial t^2} + \frac{1}{K}\frac{\partial}{\partial t}\overline{Q}(t;x,y,z) + \frac{\eta}{K}\overline{Q}(t;x,y,z)\end{aligned} \tag{31}$$

where $\overline{\mathrm{Q}}$, the concentration of charged ions, is a function of spatial coordinates and time. $K(t)$ is the diffusion coefficient and η is a constant. In the latter model, spatial derivatives must be taken in determining diffusion relaxation, which, in terms of electrical circuit analogs, lead to generalized distributed impedances (as opposed to lumped impedances) and nonlinear behavior.

Debye Relaxation

Materials having single relaxation time constants are called Debye materials. The complex permittivity in a Debye material is given by (8–10)

$$\epsilon' - j\epsilon'' = \epsilon_\infty + \frac{\epsilon_s - \epsilon_\infty}{1+\omega^2\tau^2} - j\frac{(\epsilon_s - \epsilon_\infty)\omega\tau}{1+\omega^2\tau^2} \tag{32}$$

where τ is the relaxation time, ϵ_s is the relative dielectric constant at zero frequency ($\epsilon_{dc} = \epsilon_s\epsilon_0$) and ϵ_∞ is the relative dielectric permittivity at infinite frequency. In general, apart from liquid dielectrics, single relaxations are seldom observed. Multiple relaxations or distributions of relaxations are instead found.

Generalized Relaxation Distributions

A generalized expression for material media in which multiple relaxations are found may be written as (11)

$$\epsilon' - j\epsilon'' = \epsilon_\infty + (\epsilon_s - \epsilon_\infty)\int_0^\infty \frac{D(\tau)(1-j\omega\tau)}{1+\omega^2\tau^2}\,d\tau \tag{33}$$

where $D(\tau)$ is the time-constant distribution function, normalized such that

$$\int_0^\infty D(\tau)\,d\tau = 1 \tag{34}$$

One of the most commonly observed simple relaxation distributions in lossy media is the Cole–Cole distribution. In the Cole–Cole distribution Eq. (33) reduces to

$$\epsilon' - j\epsilon'' = \epsilon_\infty + \frac{\epsilon_s - \epsilon_\infty}{1+(j\omega\tau)^{1-m}} \tag{35}$$

where $0 \le m \le 1$. The loss tangent for the Cole–Cole distribution is

$$\begin{aligned}\tan\delta &= \frac{\epsilon''}{\epsilon'} \\ &= \frac{\theta(\omega\tau)^{1-m}\sin\left[(1-m)\frac{\pi}{2}\right]}{1+\theta+(2+\theta)(\omega\tau)^{1-m}\cos\left[(1-m)\frac{\pi}{2}\right]+(\omega\tau)^{2(1-m)}}\end{aligned} \tag{36}$$

where $\theta = (\epsilon_s - \epsilon_\infty)/\epsilon_\infty$. The $m = 0$ case corresponds to a Debye material (single relaxation). The $m = 1$ case corresponds to an infinitely broad continuous distribution (one having no re-

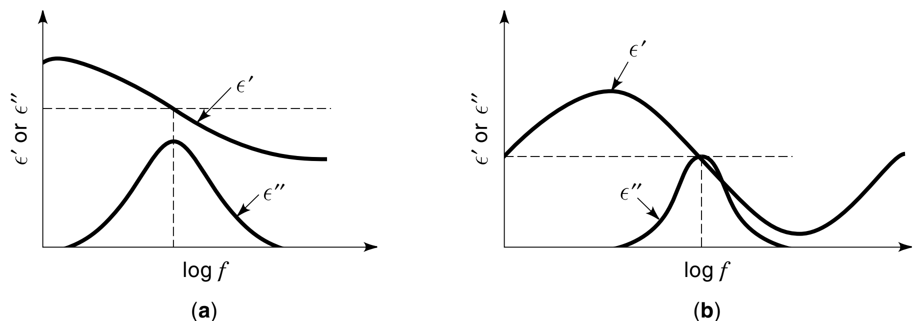

Figure 2. Two differing types of dispersion and absorption processes occuring in dielectrics as a function of frequency: (a) relaxation and (b) resonance.

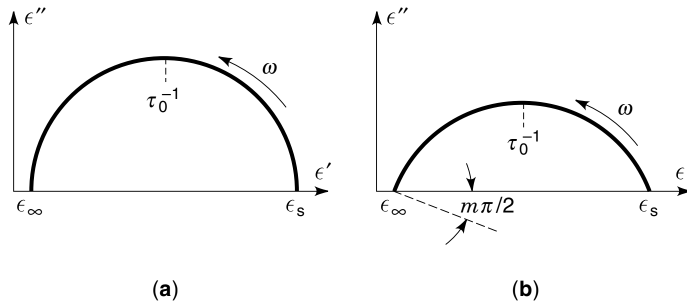

Figure 3. ϵ'' versus ϵ' plots for (a) Debye and (b) Cole–Cole materials.

laxation). In the latter case the imaginary part of the complex permittivity disappears, and the real part becomes frequency independent.

The Cole–Cole distribution corresponds to a symmetric distribution of relaxation times of width m. Whereas a Debye material yields a plot of $\epsilon''(\epsilon')$ that is a semicircle whose center lies on the $\epsilon'' = 0$ axis, a Cole–Cole $\epsilon''(\epsilon')$ plot is a semicircle whose center lies below the horizontal $\epsilon'' = 0$ axis, on a line drawn from ($\epsilon' = \epsilon_\infty$, $\epsilon'' = 0$) that makes an angle of $m\pi/2$ with the horizontal axis. This is shown in Fig. 3. In addition to the Cole–Cole expression, there are other empirical relations commonly used to describe a non-Debye response. These are the Cole–Davidson (12), the combined Cole–Cole, and the Williams–Watkins (13) expressions. A characteristic feature of all these empirical relations, besides being based on Eq. (30), is that at frequencies away from the (dominant) relaxation frequency, they reduce to expressions showing a power-law dependence (14) on frequency for both ϵ' and ϵ''.

Generalized Relation between Permittivity and Dielectric Loss Index

A generalized relation between ϵ' and ϵ'' for linear dielectric materials possessing an arbitrary number of relaxation times may be derived by regarding the permittivity as a system function characterizing the electrical properties of a material with the applied electric field as input and the displacement field as output. In the time domain the material permittivity is simply the transient (causal) system response, which can always be decomposed into the sum of an even and odd function whose Fourier transforms yield the (real) permittivity and (imaginary) dielectric loss index. The real permittivity and dielectric loss index are then related by the following Hilbert transforms, also known as the Kramers–Krönig relations,

$$\epsilon''(\omega) = \frac{1}{\pi} P \int_{-\infty}^{\infty} \frac{\epsilon'(v)}{\omega - v}\, dv \tag{37}$$

and

$$\epsilon'(\omega) = \epsilon_\infty - \frac{1}{\pi} P \int_{-\infty}^{\infty} \frac{\epsilon''(v)}{\omega - v}\, dv \tag{38}$$

where P denotes the Cauchy principal value. The application and limitations of Eqs. (37) and (38) for band-limited measurement data have been described in Ref. 11, as well as the use of an inverse power law of the distribution function for predicting expected changes in the dielectric loss tangent from measured changes in permittivity at two selected frequencies.

Effect of Temperature Changes

A classical statistical thermodynamic model using a double potential well was used (11) to describe the dispersive dielectric behavior for a bistable dielectric as a function of temperature and frequency in terms of the dipolar polarizability $\alpha_D = Np_E^2/k_BT$, the activation energy U, and the high-frequency (optical) permittivity at temperature T, where N is the total number of bistable dipoles in the material having dipole moment p_E. The results are

$$\epsilon'(\omega, T) = \epsilon_\infty(T) + \frac{\alpha_D}{1 + \omega^2\tau^2} \tag{39}$$

and

$$\tan\delta(\omega, T) = \frac{\alpha_D \omega\tau}{\alpha_D + \epsilon_\infty(T)(1 + \omega^2\tau^2)} \tag{40}$$

where $\tau = e^{-U/k_BT}/2A$ and A is a constant that may or may not depend on temperature describing the number of dipoles within the dielectric jumping per unit time from one potential energy state to a higher state. Equations (39) and (40) are limited to dielectric materials for which interaction between individual dipoles can be neglected and for conditions in which $p_E E \ll k_B T$ (nonsuperconducting states).

Langevin considered the electrostatic case of interacting molecules from a Maxwell–Boltzmann statistical ensemble average of the angular alignment with an applied electric field E of point dipoles having equal dipole moments in thermal equilibrium at temperature T. He derived the well-known Langevin function shown in Fig. 4,

$$\langle \cos\theta \rangle = \coth y - 1/y \tag{41}$$

where θ is the angle between field and dipole and y is $p_E E/(k_B T)$. The ensemble average $\langle \cos\theta \rangle$ increases with increasing y; for high values of E/T, the orienting action of the electric field dominates over the disorienting action of the temperature. Implicit in the derivation of the Langevin function are the assumptions that the molecules are *point* dipoles that have *isotropic* polarizability, that ergodicity holds, and

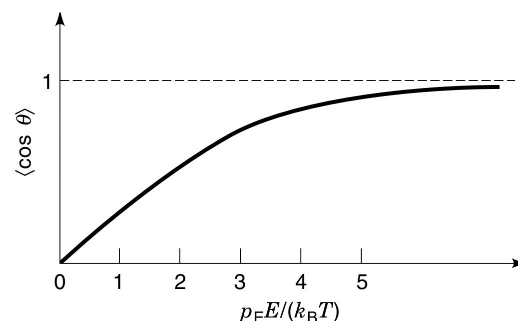

Figure 4. Behavior of Langevin function versus $p_E E/k_B T$.

that the system obeys the classical Maxwell–Boltzmann statistics.

Additional discussion on relaxation models is to be found in the classical texts of Von Hippel (15) and Böttcher (16). The use of these physical relaxation models provides insight into what dispersive permittivity and dielectric loss tangents might be expected both as a function of temperature and frequency. However, their applicability and validity must be examined by accurate measurements.

PERMITTIVITY AND DIELECTRIC-LOSS-ANGLE MEASUREMENTS

Low-Frequency Complex Impedance Measurements

The use of a plane-parallel capacitor having a vacuum capacitance $C_0 = \epsilon_0 S/h$, where S and h are, respectively, the surface area of the electrode plates and separation of the plates, is commonly used for low-frequency dielectric measurements. If a low-frequency voltage $V = V_0 e^{j\omega t}$ is applied to this capacitor, a charge $Q = C_0 V$ appears on the electrodes that is in phase with the applied voltage. The nondissipative displacement current in the external circuit is then given by

$$I = \dot{Q} = j\omega C_0 V \tag{42}$$

which is 90° out of phase with the applied voltage. If the volume between the electrodes is filled with a lossless, nonpolar insulating material, the capacitor has a capacitance $C = \epsilon_r' C_0$. In this case the new displacement current is

$$I_{\text{diel}} = \dot{Q}_{\text{diel}} = j\omega CV = \epsilon_r' I \tag{43}$$

The capacitance is larger than the vacuum capacitance, but remains 90° out of phase with respect to the applied voltage. For lossy dielectric materials, the current is not 90° out of phase with the voltage since there is a small conduction GV due to charge motion in phase with the applied voltage. If the charges are free, the conductance G is independent of frequency. However, if the charges are bound, G is frequency dependent, and the dipole relaxation phenomena previously described become relevant. In general,

$$I = (j\omega C + G)V \tag{44}$$

where $G = \sigma S/h$ (if G is the conductance due to free charges) and $C = \epsilon_r' S/h$. Whenever dissipation is not exclusively due to free charges, but is also due to bound charges, the conductivity is itself a complex frequency-dependent quantity and a distinction cannot be made between Ohmic conductivity and dielectric loss factor or between Faradaic diffusion transport and in-phase polarization.

Free-Space Measurement

Free-space measurements of the complex permittivity and complex permeability usually involve placing a plate specimen orthogonal to the axis between the transmitting and receiving antennas. A plane electromagnetic wave is passed through the specimen. The complex permittivity or permeability can then be evaluated from measurements of the propagation constant $\gamma_s = jk_s = j\omega\sqrt{\mu_0\epsilon_0\epsilon_{r,s}\mu_{r,s}}$ of the plane electromagnetic wave propagating in the specimen or from the measured impedance $Z_s = \sqrt{\mu_0\mu_{r,s}/\epsilon_0\epsilon_{r,s}}$ of the specimen. The accuracy of free-space measurements depends on the appropriate choice of a theoretical model best representing the experimental measurement system and the accuracy of the measurement system.

Solid Dielectric Specimens. For a normally incident transverse electromagnetic (TEM) wave on the specimen surrounded by air (see Fig. 5) the transmission and reflection coefficients, T_0 and R_0, are given by

$$T_0 = \frac{4\gamma_s\gamma_0}{(\gamma_0+\gamma_s)^2 e^{-\gamma_s h} - (\gamma_0-\gamma_s)^2 e^{\gamma_s h}} \tag{45}$$

$$R_0 = \frac{(\gamma_0^2-\gamma_s^2)e^{-\gamma_s h} - (\gamma_0^2-\gamma_s^2)e^{\gamma_s h}}{(\gamma_0+\gamma_s)^2 e^{-\gamma_s h} - (\gamma_0-\gamma_s)^2 e^{\gamma_s h}} \tag{46}$$

where $\gamma_0 = j2\pi/\lambda_0$ and $\gamma_s = j2\pi\sqrt{\epsilon_{r,s}\mu_{r,s}}/\lambda_0$. Equations (45) and (46) may be solved for the complex permittivity and permeability of a magnetic plane-parallel plate. If the specimen is nonmagnetic, the transmission coefficient may be solved for ϵ_r. A common reflection technique for complex permittivity evaluation is to place a conducting plate (short) behind the specimen and measure the reflection coefficient. In this case,

$$R_{0|\text{short}} = \frac{(\gamma_0-\gamma_s)e^{-\gamma_s h} - (\gamma_0+\gamma_s)e^{\gamma_s h}}{(\gamma_0+\gamma_s)e^{-\gamma_s h} - (\gamma_0-\gamma_s)e^{\gamma_s h}} \tag{47}$$

Generally, complex permittivity evaluations are more accurate in reflection (one-port scattering parameter) measurements when the specimen is surrounded by air, whereas permeability evaluations are most accurate from reflection measurements when the specimen is backed by a shorting plane.

Liquid, Gas, or Plasma Specimens. The preceding free-space experimental setup is used mainly for measuring solid dielectric specimens that have plane-parallel plate geometries. For liquids, gases, or plasmas that must be held in containers whose walls are transparent to probing electromagnetic waves, the (two-dimensional) analysis becomes somewhat more complicated (see Fig. 6). In this case the amplitude re-

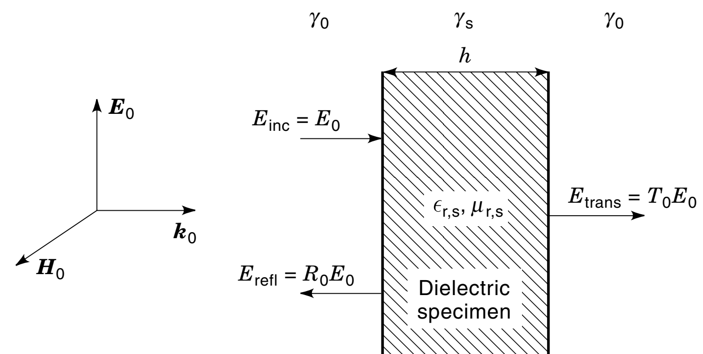

Figure 5. Reflection and transmission coefficients for an electromagnetic plane wave normally incident on an infinite dielectric plate specimen.

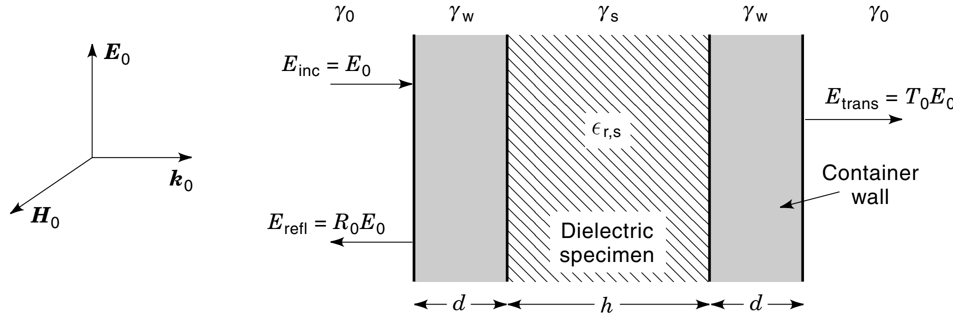

Figure 6. Free-space model for measuring liquids, gases, or plasmas in transparent container.

flection and transmission coefficients are given by (17),

$$R_0 = \frac{m\left(\dfrac{Z_s+Z_w}{Z_s-Z_w} + e^{2\gamma_w d}\dfrac{Z_w+Z_0}{Z_w-Z_0}\right) + n\left(1+e^{2\gamma_w d}\dfrac{Z_s+Z_w}{Z_s-Z_w}\dfrac{Z_w+Z_0}{Z_w-Z_0}\right)e^{2\gamma_s h}}{m\left(\dfrac{Z_s+Z_w}{Z_s-Z_w}\dfrac{Z_w+Z_0}{Z_w-Z_0} + e^{2\gamma_w d}\right) + n\left(\dfrac{Z_w+Z_0}{Z_w-Z_0} + e^{2\gamma_w d}\dfrac{Z_s+Z_w}{Z_s-Z_w}\right)e^{2\gamma_s h}} \tag{48}$$

and

$$\begin{aligned} T_0 = \Bigg\{ &\cosh(\gamma_s h)\left[\cosh^2(\gamma_w d) + \sinh^2(\gamma_w d) - \frac{1}{2}\left(\frac{Z_0}{Z_w} + \frac{Z_w}{Z_0}\right)\sinh(2\gamma_w d)\right] \\ &+ \frac{1}{2}\sinh(\gamma_s h)\left[\left(\frac{Z_s}{Z_w} + \frac{Z_w}{Z_s}\right)\sinh(2\gamma_w d) - \left(\frac{Z_s}{Z_0} + \frac{Z_0}{Z_s}\right)\cosh^2(\gamma_w d) - \left(\frac{Z_w^2}{Z_0 Z_s} + \frac{Z_0 Z_s}{Z_w^2}\right)\sinh^2(\gamma_w d)\right]\Bigg\}^{-1} \end{aligned} \tag{49}$$

where

$$m = \left(\frac{Z_0}{Z_s} + 1\right)\cosh(\gamma_w d) - \left(\frac{Z_0}{Z_w} + \frac{Z_w}{Z_s}\right)\sinh(\gamma_w d) \tag{50}$$

$$n = \left(\frac{Z_0}{Z_s} - 1\right)\cosh(\gamma_w d) - \left(\frac{Z_0}{Z_w} - \frac{Z_w}{Z_s}\right)\sinh(\gamma_w d) \tag{51}$$

and Z_0 is the free-space impedance, $Z_w = Z_0/\sqrt{\epsilon_{r,w}} = \gamma_0 Z_0/\gamma_w$ is the container wall impedance, and $Z_s = Z_0/\sqrt{\mu_{r,s}\epsilon_{r,s}} = \gamma_0 Z_0/\gamma_s$ is the impedance of the medium under test.

Waveguide Transmission-Line Methods

The use of waveguide transmission and reflection techniques for evaluating complex permittivity and complex permeability has a long history, and the literature describing various techniques is extensive (18–37). Transmission-line techniques, usually made in rectangular or coaxial waveguides, are the simplest of the relatively accurate ways of measuring permeability and permittivity. Coaxial lines are broadband in the TEM dominant mode and therefore are attractive for spectral characterization of lossy magnetic materials, despite the problems of measurement uncertainty in complex permittivity determination introduced by potential air gaps between the sample and the coaxial line center conductor. Details of two-port, reference-plane invariant scattering parameter relations that can be used for determining permittivity and permeability are given elsewhere (37). One set of equations for dielectric and magnetic measurements of a single sample, in terms of two-port scattering parameters that can be taken with an automatic network analyzer, is

$$S_{11}S_{22} - S_{21}S_{12} = \exp\left(-2\gamma_0(L_{air} - L)\right)\frac{R^2 - T^2}{1 - R^2T^2} \tag{52}$$

and

$$(S_{12} + S_{21})/2 = \exp[-\gamma_0(L_{air} - L)]\frac{T(1-R^2)}{1-R^2T^2} \tag{53}$$

where

$$R = \frac{\mu\gamma_0 - \mu_0\gamma}{\mu\gamma_0 + \mu_0\gamma} \tag{54}$$

$$T = \exp(-\gamma L) \tag{55}$$

$$\gamma_0 = \sqrt{\left(\frac{2\pi}{\lambda_c}\right)^2 - \left(\frac{\omega}{c_{lab}}\right)^2} \tag{56}$$

$$\gamma = \sqrt{\left(\frac{2\pi}{\lambda_c}\right)^2 - \frac{\omega^2\mu_r\epsilon_r}{c_{vac}^2}} \tag{57}$$

c_{vac} and c_{lab} are the speed of light in vacuum and laboratory, ω is the angular frequency, λ_c is the cutoff transmission-line wavelength, ϵ_r and μ_r are the specimen relative complex permittivity and permeability relative to vacuum, and L_{air} and L are air-line and specimen lengths. Equations (52) and (53) may be solved either explicitly or implicitly as a system of nonlinear scattering equations at each frequency or by using a nonlinear regression model over the entire frequency range. The total attenuation loss α_{TEM} of a sample under test for TEM mode structure in a coaxial transmission line is given by

$$\begin{aligned} \alpha_{TEM} &= \mathrm{Re}(\gamma) \\ &= \mathrm{Re}\left(j\frac{\omega}{c_{vac}}\sqrt{(\epsilon_r' - j\epsilon_r'')(\mu_r' - j\mu_r'')}\right) \\ &= \frac{\sqrt{2}\omega}{2c_{vac}}\sqrt{\epsilon_r'\mu_r'[(1+\tan^2\delta_e)^{1/2}(1+\tan^2\delta_m)^{1/2} + \tan\delta_e\tan\delta_m - 1]} \end{aligned} \tag{58}$$

where $\tan \delta_e = \epsilon_r''/\epsilon_r'$ and $\tan \delta_m = \mu_r''/\mu_r'$. One disadvantage of microwave measurements of the complex permittivity in waveguide is that specimens have very small tolerances in properly machined dimensions. If the specimen does not fill the entire cross section of the waveguide perfectly, corrections must be made for air gaps. For high-permittivity samples in either rectangular or coaxial transmission lines, air gaps can lead to dielectric depolarization, which yields severe underestimates of actual specimen permittivity.

Thin Film Specimens

Techniques useful for the evaluation of the dielectric properties of thin film structures are important for various applications, such as dynamic random access memory (DRAM) cells and high-frequency bypass on-chip capacitors for monolithic microwave integrated circuits (MMICs). The dielectric properties of thin film structures, commonly 8 nm to 100 nm thick, on semiconductor substrates often differ appreciably from their bulk counterparts. For example, the real permittivities of thin films are usually smaller and dielectric losses significantly larger than those of corresponding bulk materials. These differences may be due to nonuniform strain arising from film-substrate lattice mismatches, film compositional inhomogeneities, film conductivity, or other structural imperfections.

Above 1 GHz, little is known about thin film capacitive characteristics. At these frequencies measurements become more difficult as a result of stray admittance effects around the thin film deposited structure. One technique outlined in (38–40) is based on an equivalent circuit model of the capacitive on-chip test structure. The equivalent circuit is expressed by lumped elements of intrinsic capacitor admittance Y_c, and parallel and series parasitic admittance Y_p and Y_s. The measured thin film test structure has an admittance Y_t which is corrected for Y_p and Y_s to obtain the intrinsic admittance of the thin film Y_c. The parasitic admittances Y_p and Y_s are evaluated by measuring the open- and short-test circuit device admittances, Y_{open} and Y_{short}. These admittances may be determined with microwave probe station scattering parameter reflection coefficient (S_{11}) measurements. The intrinsic admittance is calculated from

$$Y_c = (Y_t - Y_{open})(Y_{short} - Y_{open})/(Y_{short} - Y_t) = G + j\omega C \quad (59)$$

where G and C are the conductance and capacitance of the intrinsic thin-film capacitor determined by the real and imaginary part of Y_c.

The dielectric loss tangent is given by

$$\tan\delta = G/(\omega C) \quad (60)$$

Resonance Methods

Resonant methods employing either closed and open cavities or dielectric resonators provide the highest measurement accuracy for evaluating complex permittivity and dielectric-loss tangent of low-loss materials at microwave frequencies (41–43). Generally, the (real) permittivity is calculated from the measured resonant frequency of one of the dominant modes of the resonant measurement system and the dimensions of the resonant structure. As long as specimen losses are low, they do not affect resonant frequencies. Exact relations between permittivity, sample dimensions, and resonant frequency exist only for simple rectangular, cylindrical, or spherical resonant structure geometries and when any permittivity inhomogeneity in the measurement fixture varies in only one of the principal coordinate directions. Resonant fixtures commonly used in practice for cylindrically shaped disk or rod specimens are shown in Fig. 7. An eigenvalue relationship, derived from Maxwell's equations and application of boundary conditions for the particular fixture of interest, always exists for a specific mode family that gives a transcendental equation relating permittivity, resonant frequency, and sample or fixture dimensions,

$$F(f_r, \epsilon_r', \text{dimensions}) = 0 \quad (61)$$

The permittivity is a numerical root of Eq. (61) for a given f_r and sample and fixture dimensions. Although there is more than one (mathematical) root to the eigenvalue equation, it is usually possible to pick the correct root, since many roots are nonphysical or the permittivity is approximately known. It is also possible, in principle, to obtain a unique solution by using two independent measurements with different mode field configurations or by using two samples having different dimensions. The resonant fixtures shown in Fig. 7 may be practically used, when properly dimensioned, for complex permittivity evaluations of low- and medium-loss materials over the frequency range 1 GHz to 50 GHz.

Several resonant fixtures of practical use possess geometries for which analytical solutions are not available. These fixtures may be analyzed with numerical mode-matching, Rayleigh–Ritz, or finite-element methods. All these techniques allow accuracy improvements by incorporating more terms in field expansions or by mesh refinement. Mode-matching (44,45) is one of the most accurate methods for computation of resonant frequencies of axially symmetric resonant fixtures. In radial mode-matching, a resonant structure is first subdivided into cylindrical regions having dielectric inhomogeneity only along the axial direction. The electromagnetic field components are then separately expanded into series modal expansions in each region. Boundary conditions that are applied at the interfaces between adjacent regions yield a system of matrix equations (with respect to the field expansion coefficients) that have nonzero solutions only when the determinant vanishes. The resonant frequencies are the values that make the determinant of the square matrix vanish.

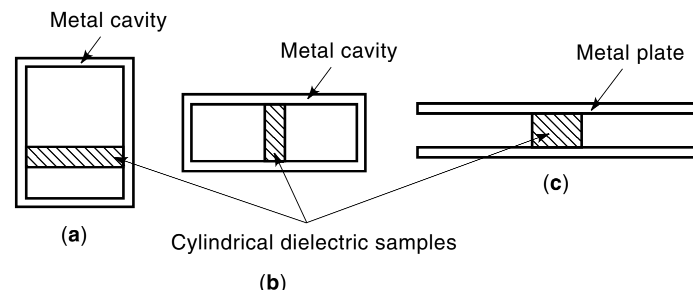

Figure 7. Typical cylindrical cavities and dielectric rod resonators used for complex permittivity measurements for which closed-form solutions are available: (a) TE_{01p} mode cavity, (b) TM_{010} mode cavity, (c) TE_{011} mode dielectric resonator.

Generally, measurement uncertainties for (real) permittivity depend on

- Presence of air gaps between the specimen and conducting parts of the resonant structure that cause depolarization [some structures are not sensitive to air gaps, such as those in Figs. 7(a) and 7(c)]
- Computational inaccuracies
- Uncertainties from physical dimensions of specimen and resonant structure

Air gaps limit the measurement accuracy of high-permittivity solid materials when the electromagnetic field structure in the measurement system has an electric field component normal to the sample surface. In these cases, a discontinuity in the normal electric field leads to depolarization. When the applied electric field is continuous across a specimen boundary, such as with cylindrical samples in TE_{0np} or quasi-TE_{0np} ($TE_{0\delta\nu}$) mode resonant fixtures (45,46), high measurement accuracies are generally achieved. In the latter case, air gaps do not play a significant role. The depolarizing effects of air gaps can be mitigated by metallization of the sample surface contacting the fixture conductors. This added procedure improves real permittivity measurement accuracy, but can substantially degrade measurement accuracy of the dielectric loss factor. When the depolarizing effects of air gaps are either not important or have been mitigated, and the numerical method used for field analysis is sufficiently accurate, real permittivity measurement uncertainty depends only on the uncertainties associated with the physical dimensions of the sample under test and the measurement system.

Evaluation of the dielectric loss index or dielectric loss tangent is always based on the expression

$$Q_{\mathrm{u}}^{-1} = p_{\mathrm{es}} \tan \delta_{\mathrm{s}} + p_{\mathrm{ed}} \tan \delta_{\mathrm{d}} + R_{\mathrm{s}}/G + Q_{\mathrm{r}}^{-1} \tag{62}$$

Equation (62) is valid for any resonant system containing isotropic dielectric materials. It defines the unloaded Q factor of the resonant system, Q_{u}, in terms of the sample partial electric energy filling factor p_{es} and sample dielectric loss tangent $\tan \delta_{\mathrm{s}}$, the electric energy filling factors of the dielectric supports p_{ed} having relative real permittivity ϵ'_{d} and loss tangent $\tan \delta_{\mathrm{d}}$ inside the resonant measurement system, the surface resistance R_{s} of any conducting shields, the geometrical factor G of the resonant system, and any radiation Q factor Q_{r} of the measurement fixture. The sample electric energy filling factor is defined as

$$p_{\mathrm{es}} = \frac{W_{\mathrm{es}}}{W_{\mathrm{et}}} = \frac{\int_{V_{\mathrm{s}}} \epsilon'_{\mathrm{r,s}} \mathbf{E} \cdot \mathbf{E}^* \, dv}{\int_V \epsilon'_{\mathrm{r}}(v) \mathbf{E} \cdot \mathbf{E}^* \, dv} \tag{63}$$

where W_{es} is the electric energy stored in the sample, W_{et} is the total electric energy stored in the resonant measurement fixture, $\epsilon'_{\mathrm{r,s}}$ is the relative real permittivity of the sample, $\epsilon'_{\mathrm{r}}(v)$ is the relative spatially dependent permittivity in the resonant structure, and the asterisk denotes complex conjugate. The electric energy filling factor for the dielectric support is given by

$$p_{\mathrm{ed}} = \frac{W_{\mathrm{ed}}}{W_{\mathrm{et}}} = \frac{\int_{V_{\mathrm{s}}} \epsilon'_{r,d} \mathbf{E} \cdot \mathbf{E}^* \, dv}{\int_V \epsilon'_r(v) \mathbf{E} \cdot \mathbf{E}^* \, dv} \tag{64}$$

where W_{ed} is the electric energy stored in the dielectric support. The geometric factor is defined by

$$G = \frac{\omega \int_V \mu_0 \boldsymbol{H} \cdot \boldsymbol{H}^* \, dv}{\int_S \boldsymbol{H}_t \cdot \boldsymbol{H}_t^* \, dS} \tag{65}$$

where H_{t} is the magnetic field tangential to any conducting shield having surface area S.

For highest accuracy in dielectric-loss tangent measurements, the first term on the right-hand side of Eq. (62) must dominate, or the last three terms on the right-hand side of Eq. (62) should be minimized and well-characterized. Evaluation of conductor losses and those due to dielectric materials other than the sample under test within the measurement system (such as dielectric supports) often requires the rigorous use of numerical computation methods. The surface resistance of metal shields must also be well-characterized at the measurement frequency and temperature of interest. If an open resonator is used, radiation losses must be considered. For most resonant measurement fixtures used in practice, uncertainties in dielectric-loss-tangent evaluations are limited by conductor losses. Conductor losses decrease as the surface resistance becomes small and as the geometric factor increases. One common procedure to minimize conductor losses is to situate the dielectric specimen in a position away from the conductor walls as shown in Fig. 8 (47–52). Usually quasi-TE_{011} modes of this structure (often called $TE_{01\delta}$ modes) are used for dielectric-loss-tangent measurements. For this mode, geometric factors approach a maximum when dimensions of the metal shield increase. The optimal value of the geometric factor (optimal positioning of the specimen relative to metal shielding) depends on sample permittivity. If the distance of the metal shield from the specimen becomes greater than the optimum value, the electric energy filling factor of the sample decreases rapidly, and the field distribution becomes essentially the same as in an empty TE_{011} cavity. With optimal shield dimensions and a metal surface resistance equal to 30 mΩ (that of copper at 10 GHz and 297 K), the Q factor due to conductor losses can be large (2×10^5 for a sample having a relative real permittivity equal to 30). Sample dielectric losses should be at least 10% of the overall losses in Eq. (62) for accurate dielectric loss measurements. Hence the lower bound on the dielectric-loss-tangent measurement is about 5×10^{-7} (for sample permittivities greater than or equal to 30) when using a $TE_{01\delta}$ mode dielectric resonator with optimal shielding conditions. For this resolution, the geometric factor must be accurately known. Another way to minimize conductor losses is to employ high-temperature superconductors as the shielding material (53–55); however, this can only be done at cryogenic temperatures.

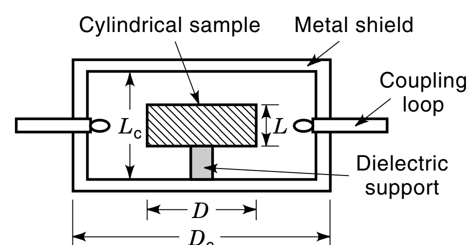

Figure 8. $TE_{01\delta}$ mode dielectric resonator measurement fixture.

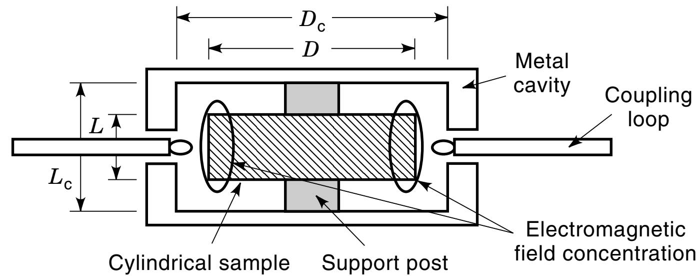

Figure 9. Whispering-gallery mode resonant structure.

The most effective way to decrease conductor losses (or increase the geometric factor) for accurate dielectric-loss-tangent measurements is to use higher-order hybrid modes having high azimuthal mode numbers. These hybrid modes, called *whispering-gallery modes,* are excited in cylindrical specimens (56) as shown in Fig. 9. Conductor losses decrease very rapidly with increasing azimuthal mode numbers for whispering-gallery modes. Therefore they can be used for high-resolution dielectric-loss-tangent measurements of ultralow-loss materials. In addition, this method can be used for measurements of low-dielectric-loss materials up to frequencies of 100 GHz.

The most commonly used dielectric materials in the electronics industry are those used for printed wiring board substrates. Typically these dielectric materials exhibit losses in the range, $10^{-4} < \tan\delta < 10^{-2}$. Because printed wiring board substrates are relatively thin dielectric sheets, the resonant measurement techniques described previously are not applicable. For these samples the most convenient measurement technique is the split (tuned) dielectric post resonator illustrated in Fig. 10. This nondestructive method can be used practically at all frequencies from 1 GHz to 10 GHz.

When measurement frequencies lower than 1 GHz are of interest, dimensions of the resonant structures described thus far become impractically large. One of the commonly used resonant structures when dielectric measurements are required in the frequency range between 100 MHz and 1 GHz is the reentrant cavity, which is shown in Fig. 11. Advantages in the use of the reentrant cavity are relatively small sample size and, because of the axially directed electric field, a permittivity measurement normal to the substrate laminar surfaces. However, the reentrant cavity technique is sensitive to the presence of air gaps between the sample and the central metal posts, so that without metallization of the top and bottom surfaces of the specimen, it is only useful for measurements of low- to medium-permittivity materials.

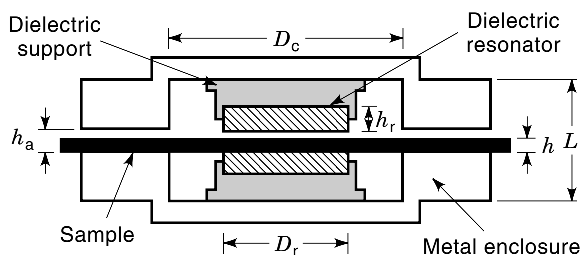

Figure 10. Split post-dielectric resonator.

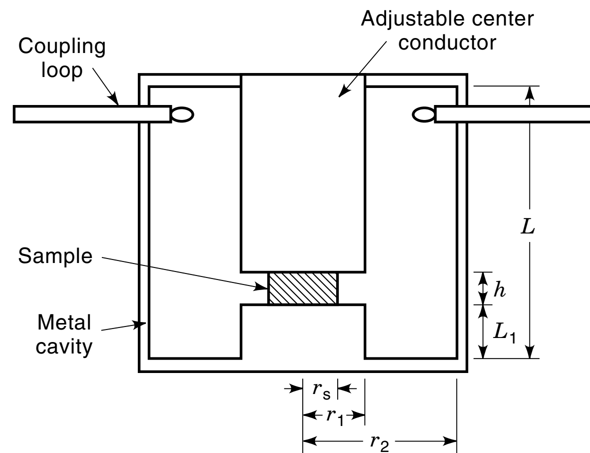

Figure 11. Doubly reentrant cavity.

At frequencies above 50 GHz, the dimensions of the resonant structures become impractically small. At these frequencies, a typical method (see Fig. 12) for complex permittivity measurements is the semiconfocal Fabry–Perot type resonator (56), although for very-low-loss materials, the whispering-gallery mode technique could also be used (57). Free-space transmission and reflection techniques previously described can also be used to characterize materials from 50 GHz to visible-light frequencies.

Complex Permittivity Measurements of Anisotropic Materials. Many materials, including some single crystals, exhibit dielectric anisotropy. For dielectrically anisotropic materials the complex permittivity is not independent of direction. The general (diagonalized) form of the electric susceptibility tensor is given in Eq. (7).

Anisotropy is usually related to the internal structure of the material. It can also be enforced by external factors, such as an external static magnetic field or mechanical stress. For anisotropic materials the relationship between the electric field intensity vector $\boldsymbol{E}$ and electric flux density vector $\boldsymbol{D}$ takes the form

$$\boldsymbol{D} = \overline{\overline{\epsilon}} \cdot \boldsymbol{E} = \begin{bmatrix} \epsilon_{11} & \epsilon_{12} & \epsilon_{13} \\ \epsilon_{21} & \epsilon_{22} & \epsilon_{23} \\ \epsilon_{31} & \epsilon_{32} & \epsilon_{33} \end{bmatrix} \begin{bmatrix} E_1 \\ E_2 \\ E_3 \end{bmatrix} \tag{66}$$

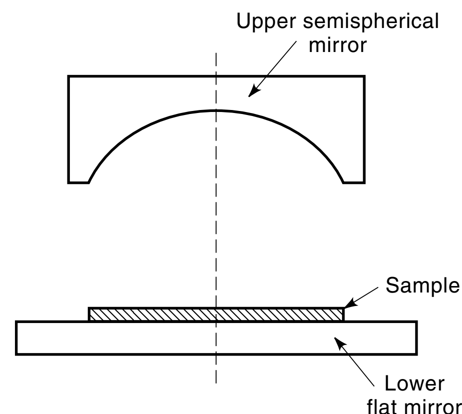

Figure 12. Fabry–Perot semiconfocal resonator.

where the complex permittivity $\overline{\overline{\epsilon}}$ is a second-rank tensor. The permittivity tensor may generally be expressed as a sum of symmetric and antisymmetric tensors

$$\overline{\overline{\epsilon}} = \overline{\overline{\epsilon}}^{(S)} + \overline{\overline{\epsilon}}^{(A)} \tag{67}$$

For the symmetric tensor, $\epsilon_{ij}^{(S)} = \epsilon_{ji}^{(S)}$ and for the antisymmetric tensor, $\epsilon_{ij}^{(A)} = -\epsilon_{ji}^{(A)}$. The Hermitian and anti-Hermitian parts of the permittivity tensor are

$$\overline{\overline{\epsilon}}' = \frac{1}{2}(\overline{\overline{\epsilon}} + \overline{\overline{\epsilon}}_t^*) \tag{68}$$

$$\overline{\overline{\epsilon}}'' = \frac{1}{2}j(\overline{\overline{\epsilon}} - \overline{\overline{\epsilon}}_t^*) \tag{69}$$

where $\overline{\overline{\epsilon}}_t^*$ represents the complex conjugate of the transposed tensor. The Hermitian part of the permittivity tensor is associated with electric energy stored in the dielectric while the anti-Hermitian part represents power dissipation in the dielectric. Most dielectric materials are described by a symmetric tensor only and dielectric losses by the imaginary components of a symmetric tensor. For a symmetric tensor there is always a coordinate system in which the permittivity tensor may take the diagonalized form,

$$\overline{\overline{\epsilon}} = \begin{bmatrix} \epsilon_{11} & 0 & 0 \\ 0 & \epsilon_{22} & 0 \\ 0 & 0 & \epsilon_{33} \end{bmatrix} \tag{70}$$

When single crystals are measured, the coordinate axes are associated with the principal axes of the crystal lattice. When two of the three components of the permittivity tensor are equal, the material is said to be uniaxially anisotropic.

The easiest approach to measuring complex permittivity of anisotropic materials is to use measurement fixtures in which there is only one component of the electric field in the sample under test. For example, in the reentrant cavity and TM_{010} cylindrical cavity, there is only an axial electric field component in the specimen. In coaxial transmission line, only a radial electric field component is present when operating in dominant TEM mode field structure and in a TE_{01n} cavity, there is only an azimuthal electric field component in the specimen. If the specimen is properly oriented using one of these measurement techniques, measurement data can be obtained for evaluation of all tensor permittivity components.

For uniaxially anisotropic materials, a cylindrical specimen is first oriented so that the cylinder axis is parallel to the anisotropy axis of the material. Then a reentrant cavity can be used to evaluate the complex permittivity parallel to the anisotropy axis. If the sample specimen is measured in a TE_{01n} mode cavity, the permittivity perpendicular to the anisotropy axis can be determined. For general (orthogonal) three-dimensional anisotropy, a rectangular waveguide sample may be fabricated so that the principal anisotropy axes are parallel to the Cartesian axes, or three cylindrical specimens can be fabricated the cylindrical axes of which are oriented parallel to each of the different anisotropy axes. In general, three independent measurements are required for evaluation of the permittivity tensor. This can be accomplished with two or three differently oriented samples or with the use of two or three different modes using only one sample.

It is preferable, but not necessary, that only one permittivity tensor component be excited by the electric field structure in the measurement fixture. However, this is not always possible, since other factors, such as sensitivity and measurement accuracy, must also be considered.

Many single crystals have extremely low dielectric loss at low temperature (58–62). It is possible to evaluate dielectric losses in these extremely low-loss materials only by using resonant fixtures in which conductor losses are very small. For these measurements the whispering-gallery mode technique is appropriate. Whispering-gallery modes can always be classified into modes symmetric (S) or antisymmetric (N) to a plane of symmetry in a measurement fixture. In fact, since for these modes the electromagnetic fields are well confined to the dielectric specimen, this classification can still be made relative to the specimen's equatorial plane even if the resonant fixture does not have a symmetry plane. To evaluate the principal permittivity components of a uniaxially anisotropic dielectric resonator, a specimen whose cylindrical axis is along a principal direction of anisotropy is first obtained. Then two whispering-gallery mode resonances that exhibit a quasi-TE (H mode) and quasi-TM (E mode) field structure are identified and measured. Finally, a system of two nonlinear determinant equations are solved with respect to the two unknown permittivity tensor components,

$$\begin{aligned} F_1(f^{(H)}, \epsilon_\perp, \epsilon_\parallel) = 0 \\ F_2(f^{(E)}, \epsilon_\perp, \epsilon_\parallel) = 0 \end{aligned} \tag{71}$$

where $f^{(H)}$ and $f^{(E)}$ are the measured resonant frequencies for the quasi-TE (H) and the quasi-TM (E) whispering gallery modes and $\epsilon_\perp$ and $\epsilon_\parallel$ are the real parts of the permittivity tensor components normal and parallel to the anisotropy axis. The eigenvalue equations represented by F_1 and F_2 result from application of variational or mode-matching methods. Once the real permittivities are evaluated from Eq. (71), dielectric-loss tangents can be computed as solutions to

$$\begin{aligned} Q_E^{-1} = p_{e\perp}^{(E)} \tan\delta_\perp + p_{e\parallel}^{(E)} \tan\delta_\parallel + R_s/G^{(E)} \\ Q_{(H)}^{-1} = p_{e\perp}^{(H)} \tan\delta_\perp + p_{e\parallel}^{(H)} \tan\delta_\parallel + R_s/G^{(H)} \end{aligned} \tag{72}$$

where $\tan\,\delta_\perp$ and $\tan\,\delta_\parallel$ are the dielectric-loss tangents perpendicular and parallel to the anisotropy axis; $p_{e\perp}^{(H)}$, $p_{e\parallel}^{(H)}$, $p_{e\perp}^{(E)}$, $p_{e\parallel}^{(E)}$ are the electric energy filling factors perpendicular and parallel to the anisotropy axis of the dielectric resonator for quasi-TM whispering-gallery modes (superscript E) and quasi-TE whispering gallery modes (superscript H); and $G^{(E)}$ and $G^{(H)}$ are the geometric factors for quasi-TM and quasi-TE whispering-gallery modes.

Table 1 shows permittivity and dielectric-loss-tangent-measurement results for single-crystal sapphire at room temperature and at 4.2 K using whispering-gallery modes. The electric energy filling factors in Table 1 show that both N1 and S2 mode families can be treated as quasi-TM and quasi-TE modes. The geometric factor calculations demonstrate that conductor losses are considerably smaller than dielectric losses for large azimuthal mode numbers and can be neglected in most cases. Hence the dielectric-loss tangents can be approximated as the reciprocals of the unloaded Q factors for quasi-TM and quasi-TE whispering-gallery modes. Permittivities were evaluated accounting for thermal expansion

Table 1. Electric energy filling factors, geometric factors and measured loss tangents using several quasi-TM (N1) and quasi-TE (S2) modes of the sapphire resonator. Sapphire specimen, having diameter of 50.02 mm and height of 30.03 mm, in metallic shield having 80 mm diameter and 50 mm height. Computed permittivity tensor components: $\epsilon_\perp$ = 9.27 and $\epsilon_\|$ = 11.35 at 4.2 K and $\epsilon_\perp$ = 9.40 and $\epsilon_\|$ = 11.59 at 296.5 K.

Type	m	$p_{e\perp}$	$p_{e\|}$	$G(\Omega)$	tan δ	
					4.2 K	296.5 K
N1	11	0.0470	0.9341	6.77×10^6		5.0×10^{-6}
	12	0.0402	0.9423	1.63×10^7	5.0×10^{-9}	4.8×10^{-6}
	13	0.0350	0.9488	3.92×10^7	1.0×10^{-9}	4.8×10^{-6}
	14	0.0303	0.9538	9.42×10^7	7.0×10^{-10}	5.0×10^{-6}
S2	10	0.9548	0.0103	6.04×10^6	5.0×10^{-9}	9.0×10^{-6}
	11	0.9607	0.0064	1.60×10^7	4.0×10^{-9}	9.0×10^{-6}
	12	0.9620	0.0081	4.20×10^7	2.0×10^{-9}	7.0×10^{-6}
	13	0.9585	0.0106	1.10×10^8	9.0×10^{-10}	7.0×10^{-6}

coefficients (63,64). At 4.2 K, conductor losses for the copper metal shield used in experiments can be neglected only for azimuthal mode numbers $m > 13$. Conductor losses for whispering-gallery mode dielectric resonators can be made negligible by either performing measurements on higher-order azimuthal modes or by simply enlarging the enclosing metal shield.

BIBLIOGRAPHY

1. J. D. Jackson, *Classical Electrodynamics,* New York: Wiley, 1975.
2. A. Nussbaum, *Electromagnetic and Quantum Properties of Materials,* Englewood Cliffs, NJ: Prentice-Hall, 1966.
3. J. C. Maxwell, *A Treatise on Electricity and Magnetism,* New York: Dover, 1891.
4. K. W. Wagner, Erklarung der dielectrischen Nachwirkungs worgange auf Grund Maxwellscher, *Arch. Electrotechnik,* **20**: 371, 1914.
5. R. W. P. King and G. S. Smith, *Antennas in Matter,* Cambridge, MA: MIT Press, 1981.
6. S. S. Dukhin, Dielectric properties of disperse systems, in E. Matijevic (ed.), *Surface and Colloid Science,* Vol. 3, New York: Wiley-Interscience, 1969.
7. R. G. Geyer, J. Mantese, and J. Baker-Jarvis, Effective medium theory for ferrite-loaded materials, *Natl. Inst. Stand. Technol. Tech. Note 1371,* 1994.
8. J. B. Hasted, *Aqueous Dielectrics,* London: Chapman & Hall, 1973.
9. P. Debye, *Polar Molecules,* New York: Chemical Catalog, 1929.
10. C. P. Smyth, *Dielectric Relaxation and Molecular Correlation in Dielectric and Related Molecular Processes,* London: Chemical Soc., 1966.
11. R. G. Geyer, Dielectric characterization and reference materials, *Natl. Inst. Stand. Technol. Tech. Note 1338,* 1990.
12. K. S. Cole and R. H. Cole, Dispersion and absorption in dielectrics, *J. Chem. Phys.,* **9**: 341–351, 1941.
13. G. Williams and D. C. Watts, Non-symmetrical dielectric relaxation behavior arising from a simple empirical decay function, *Trans. Faraday Soc.,* **66**: 80–85, 1970.
14. A. K. Jonscher, *The universal dielectric response, a review of data and their new interpretation,* Chelsea Dielectric Group, Univ. London, 1979.
15. A. Von Hippel, *Dielectrics and Waves,* New York: Wiley, 1954.
16. C. J. Böttcher, *Theory of Electric Polarization,* Vols. 1 and 2, New York: Elsevier, 1978.
17. J. Musil and F. Zacek, *Microwave Measurements of Complex Permittivity by Free Space Methods and Their Applications,* New York: Elsevier, 1986.
18. S. Roberts and A. Von Hippel, A new method for measuring dielectric constant and loss in the range of centimeter waves, *J. Appl. Phys.,* **7**: 610–616, 1946.
19. N. Marcuvitz, *Waveguide Handbook,* New York: Dover, 1951.
20. G. A. Deschamps, Determination of reflection coefficients and insertion loss of a waveguide junction, *J. Appl. Phys.,* **2**: 1046–1050, 1953.
21. D. M. Bowie and K. S. Kelleher, Rapid measurement of dielectric constant and loss tangent, *IEEE Trans. Microwave Theory Tech.,* **MTT-4**: 137–140, 1956.
22. M. Sucher and J. Fox (eds.), *Handbook of Microwave Measurements,* Polytechnic Inst. Brooklyn Series, New York: Wiley, 1963.
23. H. E. Bussey and J. E. Gray, Measurement and standardization of dielectric samples, *IRE Trans. Instrum.,* **I-11**: 162–165, 1962.
24. G. M. Brydon and D. J. Hepplestone, Microwave measurements of permittivity and tan δ over the temperature range 20–700°C, *Proc. Inst. Elec. Eng.,* **112**: 421–425, 1965.
25. G. Franceschetti, A complete analysis of the reflection and transmission methods for measuring the complex permeability and permittivity of materials at microwave frequencies, *Alta Frequenzia,* **36**: 757–764, 1967.
26. A. M. Nicolson and G. F. Ross, Measurement of the intrinsic properties of materials by time domain techniques, *IEEE Trans. Instrum. Meas.,* **IM-19**: 377–382, 1970.
27. W. B. Weir, Automatic measurement of complex dielectric constant and permeability at microwave frequencies, *Proc. IEEE,* **62**: 33–36, 1974.
28. S. Stuchly and M. Matuszewski, A combined total reflection transmission method in application to dielectric spectroscopy, *IEEE Trans. Instrum. Meas.,* **IM-27**: 285–288, 1978.
29. M. S. Freeman, R. N. Nottenburg, and J. B. DuBow, An automated frequency domain technique for dielectric spectroscopy of materials, *J. Phys. E,* **12**: 899–903, 1979.
30. L. P. Ligthardt, A fast computational technique for accurate permittivity determination using transmission line methods, *IEEE Trans. Microw. Theory Tech.,* **MTT-31**: 249–254, 1983.
31. Hewlett Packard Product Note 8510-3, *Measuring dielectric constant with the HP 8510 network analyzer,* Palo Alto, CA: Hewlett-Packard, 1985.
32. L. Solymar and D. Walsh, *Lectures on Electrical Properties of Materials,* London: Oxford Univ. Press, 1988.
33. N. Belhadj-Tahar, A. Fourier-Lamer, and H. de Chanterac, Broadband simultaneous measurement of complex permittivity

and permeability using a coaxial discontinuity, *IEEE Trans. Microw. Theory Tech.,* **2**: 1–7, 1990.

34. K. E. Mattar and M. E. Brodwin, A variable frequency method for wide-band microwave material characterization, *IEEE Trans. Instrum. Meas.,* **39**: 609–614, 1990.
35. H. B. Sequeira, Extracting μ_r and ϵ_r from one-port phasor network analyzer measurements, *IEEE Trans. Instrum. Meas.,* **39**: 621–627, 1990.
36. G. Maze, J. L. Bonnefoy, and M. Kamarei, Microwave measurement of the dielectric constant using a sliding short-circuited waveguide method, *Microw. J.,* **33** (10): 77–88, 1990.
37. J. Baker-Jarvis et al., Transmission/reflection and short-circuit line methods for measuring permittivity and permeability, *Natl. Inst. Stand. Technol. Note 1355-R,* 1993.
38. K. Ikuta, Y. Umeda, and Y. Ishii, Measurement of high-frequency characteristics in the mm-wave band for dielectric thin films on semiconductor substrates, *Jpn. J. Appl. Phys.,* **34**, part 2 (9B): 1211–1213, 1995.
39. J. D. Banieki et al., Dielectric relaxation of $Ba_{0.7}Sr_{0.3}TiO_3$ thin films from 1 MHz to 20 GHz, *Appl. Phys. Lett.,* **72** (4), 498–500, 1998.
40. W. Williamson III et al., High frequency dielectric properties of PLZT thin films, *Integrated Ferroelectrics,* **17,** 197–203, 1997.
41. E. J. Vanzura, R. G. Geyer, and M. D. Janezic, The NIST 60-millimeter cylindrical cavity resonator: performance evaluation for permittivity measurements, *Natl. Inst. Stand. Technol. Note 1354,* 1993.
42. R. G. Geyer, L. Sengupta, and J. Krupka, Microwave properties of composite ceramic phase shifter materials, *IEEE Proc. 10th Int. Symp. Appl. Ferroelectrics,* 1996, pp. 851–854.
43. R. G. Geyer, C. Jones, and J. Krupka, Microwave characterization of dielectric ceramics for wireless communications, in *Advances in Dielectric Ceramic Materials,* Am. Ceram. Soc. Trans., **88**: 75–91, 1998.
44. Sz. Maj and M. Pospieszalski, A composite multilayered cylindrical dielectric resonator, *IEEE MTT-S Int. Microw. Symp. Dig.,* 1984, pp. 190–192.
45. D. Kajfez and P. Guillon, *Dielectric Resonators,* Chap. 6, Dedham, MA: Artech House, 1986.
46. W. E. Courtney, Analysis and evaluation of a method of measuring the complex permittivity and permeability of microwave insulators, *IEEE Trans. Microw. Theory Tech.,* **18**: 476–485, 1970.
47. Y. Kobayashi, N. Fukuoka, and S. Yoshida, Resonant modes for a shielded dielectric road resonator, *Electron. and Commun. (Japanese),* **64-B**: 46–51, 1981.
48. Y. Kobayashi, Y. Aoki, and Y. Kabe, Influence of conductor shields on the Q-factors of a TE_0 dielectric resonator, *IEEE MTT-S Int. Microw. Symp. Dig.,* 1985, pp. 281–284.
49. J. Krupka, Resonant modes in shielded cylindrical and single-crystal dielectric resonators, *IEEE Trans. Microw. Theory Tech.,* **37**, 691–697, 1989.
50. *Dielectric Resonators—A Designer Guide to Microwave Dielectric Ceramics,* Trans-Tech Inc. Pub. No. 50080040, Rev. 2, 1990.
51. Y. Kobayashi and T. Senju, Resonant modes in shielded uniaxial-anisotropic dielectric rod resonator, *IEEE Trans. Microw. Theory Tech.,* **41**: 2198–2205, 1993.
52. J. Krupka and A. Kedzior, Optimization of the complex permittivity measurement of low loss dielectrics in a cylindrical TE_{01n} mode cavities, *Electron Technol.,* **14**: 67–79, 1981.
53. J. Krupka et al., Dielectric properties of single crystals of Al_2O_3, $LaAlO_3$, $NdGaO_3$, $SrTiO_3$, and MgO at cryogenic temperatures, *IEEE Trans. Microw. Theory Tech.,* **42**: 1886–1890, 1993.
54. R. G. Geyer and J. Krupka, Microwave dielectric properties of anisotropic materials at cryogenic temperatures, *IEEE Trans. Instrum. Meas.,* **44**: 329–331, 1995.
55. H. Takamura, H. Matsumoto, and K. Wakino, Low temperature properties of microwave dielectrics, *Proc. 7th Meeting Ferroelectric Materials Their Applications, Jpn. J. Appl. Phys., Suppl. 28-2,* **28**: 21–23, 1989.
56. A. L. Cullen and P. K. Yu, The accurate measurement of permittivity by means of an open resonator, *Proc. R. Soc. London, Ser. A,* **325**: 493–509, 1971.
57. J. Krupka et al., Study of whispering gallery modes in anisotropic single-crystal dielectric resonators, *IEEE Trans. Microw. Theory Tech.,* **42**: 56–61, 1994.
58. V. Braginsky, V. S. Ilchenko, and Kh. S. Bagdassarov, Experimental observation of fundamental microwave absorption in high quality dielectric crystals, *Phys. Lett. A,* **120**: 300–305, 1987.
59. R. Shelby and J. Fontanella, The low temperature electrical properties of some anisotropic crystals, *J. Phys. Chem. Solids,* **41**: 69–74, 1980.
60. M. E. Tobar and A. G. Mann, Resonant frequencies of higher order modes in cylindrical anisotropic resonators, *IEEE Trans. Microw. Theory Tech.,* **39**: 2077–2083, 1991.
61. A. N. Luiten, A. G. Mann, and D. G. Blair, Paramagnetic susceptibility and permittivity measurements at microwave frequencies in cryogenic sapphire resonators, *J. Phys. D,* **29**: 2082–2090, 1996.
62. R. G. Geyer, J. Krupka, and M. Tobar, Microwave dielectric properties of low-loss materials at low temperature, *Proc. Mater. Res. Soc. Hybrid Mater.,* 1998.
63. C. A. Swenson, R. B. Roberts, and G. K. White, Thermophysical properties of some key solids, in G. K. White and M. L. Minges (eds.), *CODATA Bulletin 59,* Chap. 4, New York: Oxford Pergamon, 1985.
64. G. K. White, Reference materials for thermal expansion: Certified or not, *Thermochim. Acta,* **218**: 83–99, 1993.

JERZY KRUPKA
Instytut Mikroelektroniki i Optoelektroniki Politechniki Warszawskiej
RICHARD G. GEYER
National Institute of Standards and Technology

LOSSES, INSURED. See INSURANCE.
LOSSY IMAGE COMPRESSION. See IMAGE CODES.
LOSSY VIDEO COMPRESSION. See IMAGE CODES.
LOW FREQUENCY SKY WAVE PROPAGATION. See SKY WAVE PROPAGATION AT LOW FREQUENCIES.
LOW-NOISE AMPLIFIERS. See PREAMPLIFIERS.
LOW-NOISE DESIGN. See CIRCUIT NOISE.
LOW-NOISE RECEIVERS. See UHF RECEIVERS.